Autonomous monopile inspection in a turbulent wake

Bas J. de Kruif
Maritime Research Institute Netherlands
Wageningen, The Netherlands
b.j.d.kruif@marin.nl

Artur K. Litdke
Maritime Research Institute Netherlands
Wageningen, The Netherlands
a.lidtke@marin.nl

***Abstract*—Frequent underwater inspections are required to ensure the integrity of offshore infrastructure. These inspections currently rely on large vessels, Remotely Operated Vehicles (ROVs), and divers, making them dangerous, costly as well as labour- and emission-intensive. Autonomous Underwater Vehicles (AUVs) offer a more efficient approach to carry out these tasks. However, the AUVs are subjected to harsh environmental conditions and turbulent flows, which degrade the tracking performance to such an extent that the inspection sensors cannot provide adequate measurements.**

This study investigates whether information from a previous circumnavigation around a monopile can improve the tracking performance during subsequent passes. This is tested for a monopile in a 0.5 m/s current, which results in a turbulent wake on the leeward side. A Repetitive Control approach has been employed for this purpose.

The tracking error was significantly reduced with this approach. The error in the distance the camera perceives decreased from 0.46 m to one centimetre, and the heading maximum absolute error improved from 21° to 1°, which shows that previous information can indeed be used to improve the behaviour. The remaining errors are attributed to the stochastic nature of the turbulence. The next step is to improve the sensor and thruster modelling, which was not included in this study.

***Index Terms*—Monopile inspection, Turbulent flow, Repetitive Control, Autonomous Underwater Vehicle.**

I. Introduction

The Dutch North Sea is becoming more and more congested. Installed offshore wind capacity is projected to grow from 2.3 GW today to over 21 GW by 2031, implying at least 15 new turbine turbine parks with thousands of new units [1]. Ensuring the operational integrity of the related offshore infrastructure, such as monopiles and mooring lines, requires frequent and reliable underwater inspections. Current inspection methods rely heavily on large vessels, remotely operated vehicles (ROV), and divers. This makes them costly, labour- and emission-intensive, as well as constrained by the limited availability of specialised personnel.

Autonomous Underwater Vehicles (AUVs) offer an efficient approach to inspect maritime infrastructure [2]. The AUV should autonomously manoeuvre close to the structure, at 1 m distance, and assess its integrity by taking high-resolution pictures or deploying other sensing techniques. Such an operation requires that the distance from the camera to the infrastructure is tracked with high precision.

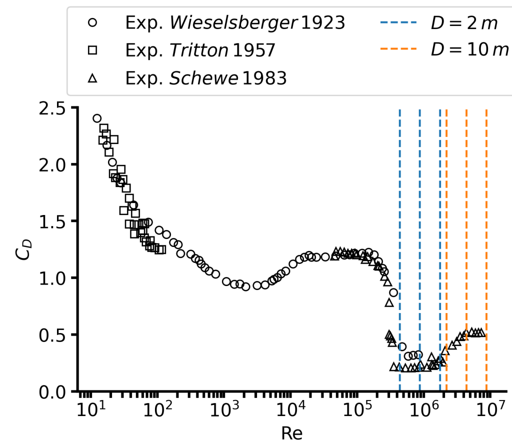

Fig. 1: Drag coefficient of a circular cylinder versus Reynolds number ($Re = DU/\nu$). Reynolds numbers for representative diameters D of 2 and 10 m and current speeds between 0.25 and 1.00 m/s are indicated as dashed lines.

Inspections are currently done mostly at dead-tide such that tidal currents acting on the deployed assets are minimal. The inspection process could be made more cost-effective if it were extended to less favourable conditions with tidal-current and waves. The flow field around offshore structures is highly turbulent even at moderate current speeds, as evident from Fig. 1. The figure shows that for typical monopile dimensions and current speeds, the flow regime is beyond the drag crisis. This leads to the formation of a turbulent wake on the leeward side. The effect of this on AUV control was previously investigated in [3] which showed that a substantial amount of actuation is required to compensate for the resultant disturbances induced by the fluctuating velocity distributions in the wake of the structure that the AUV needs to navigate. This makes ordinary disturbance-observer based controllers sub-optimal, as they typically assume a constant or slowly varying disturbance [4]. The work of [5] shows the use of Sliding Mode Control to counter disturbance while cleaning underwater infrastructure. Its aim to maintaining position, and not to survey the monopile.

The aim of this work is to investigate whether disturbance information can be collected by the AUV during each circum-

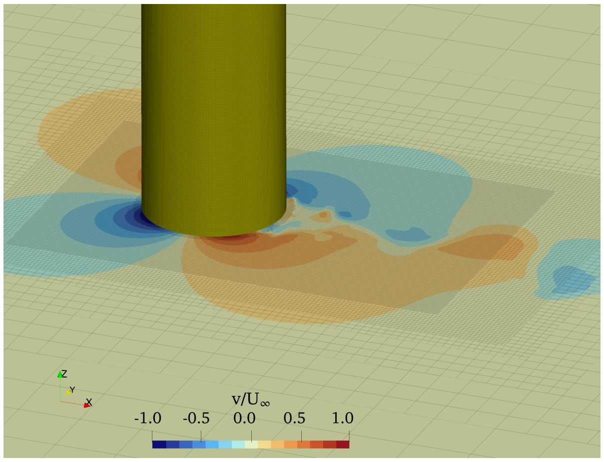

Fig. 2: Computational grid used for the scale-resolving simulations of the flow past the monopile.

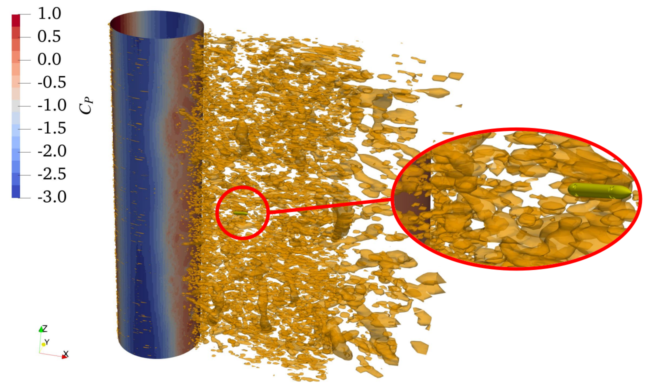

Fig. 3: Flow around a 10 m monopile immersed in a 0.5 m/s current flowing from left to right. Contours on the monopile indicate the pressure coefficient. The orange volume iso-contour shows the Q criterion value of 0.5, which indicates regions in the flow where rotation dominates the strain rate, highlighting coherent turbulent structures in the wake of the cylindrical structure. These may be seen to have similar characteristic length to that of the vehicle. Note: mAUV was not included in the CFD simulations and is only placed in the figure for visualization purposes.

navigation, and then include it into controller signal of the next circumnavigation to improve the tracking performance. To this end, a feedback controller is used to counter stochastic disturbances of the turbulent wake, while a feed forward controller learns to compensate the reproducible component of it. The approach used is Repetitive Control (RC) that assumes the duration of each circumnavigation of the target structure to be constant [6].

The paper starts by describing the simulation environment used in this study. It encompasses the turbulent wake modelling and a description of the vessel's dynamics. In section III the feedback and feed forward controllers are designed and the results are treated in section IV. The results are discussed in the final section and future research directions are identified.

II. Simulation environment

A. Problem definition

For the current study, a simple monopile, typically used on offshore wind turbines, has been chosen as an object to be inspected. Focus of the analysis has been put on capturing the effects of the turbulent flow while the action of waves has been ignored to simplify the problem statement. Typical sizes of monopile diameters seen in practice for offshore wind turbines range between 1 and 10 m [7], [8] and extreme current speeds in the Dutch North Sea can reach up to 1 m/s over the service life of currently installed assets [9]. These parameters correspond to a Reynolds number of the order of 10^6 and above, which is well beyond the drag crisis, as shown in Fig. 1. To narrow down the scope of this study, a monopile with a diameter of 10 m and a current speed of 0.5 m/s is considered, which corresponds to a Reynolds number of approximately $5 \cdot 10^6$.

Scale-resolving simulations have been used to simulate the turbulent flow past the structure, focusing on capturing the turbulent flow in the wake. CFD has carried out with ReFRESCO, a finite volume solver developed by Marin. Partially Averaged Navier-Stokes (PANS) tubulence modelling was employed, following previous application to bluff body flows at intermediate and high Reynolds numers [10], [11].

Computational grid used for the computations is shown in Fig. 2. This was wall-resolved in the wall-normal direction and refined up to 2D downstream and 1D laterally to capture the main flow structures in the wake. In order to reduce the computational cost, the spanwise extent was limited to 4D and the axial and spanwise resolution was kept coarser than would be required for fully-resolved LES, taking advantage of the PANS approach. This can be further justified by the fact that the AUV simulations were carried out only on a single plane, making it less critical to capture full detail of the 3D flow, especially in the spanwise direction. The total grid size was approximately 10 million cells. Second order time and spatial discretisation was used. More detail on the numerical approach are given in [11].

For the chosen condition, the dominant vortex shedding period corresponded to approximately 100 s. Therefore, flow data has been collected at a frequency of 2 Hz, thus approximately at 50 samples per shedding cycle. This was done over several shedding cycles after the initial transient to ensure that the flow field is sufficiently developed and data is statistically converged.

An example flow field around a 10 m monopile with the mAUV in its wake is shown in Fig. 3. It may be seen that the flow is turbulent, with large coherent structures in the wake of the monopile. These have similar characteristic length to that of the vehicle, which makes them relevant for the control problem at hand. The pressure distribution on the monopile

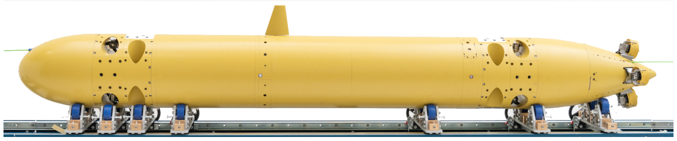

(a) Photo of the MAUV

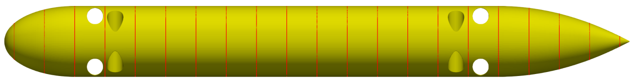

(b) Cross-flow drag strips used in cross-flow drag computation

Fig. 4: The in-house developed MAUV used in the simulations.

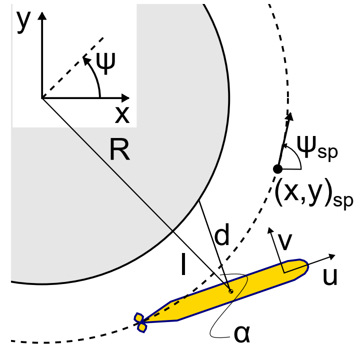

Fig. 5: The East-North-Up coordinate system used in this work. The variables are referred to in the text.

is also non-uniform, which leads to a complex mean force distribution on the AUV as it moves through the wake.

B. AUV *dynamics model*

The AUV under consideration is the in-house developed MAUV [12]. It is a 3.1 m long torpedo shaped fully-actuated AUV with a diameter of 0.35 m. The bow is elliptical shaped and the aft parabolic. A photo of the AUV is shown in Fig. 4.

The simulations were performed using MARIN's in-house sea keeping and manoeuvring simulation code aNySIM; a time-domain tool that solves the vessel's 6 DOF equations of motion [13]. The coordinate system used is shown in Fig. 5. Only the yaw, surge and sway motions are used in this study. Control signals are calculated in Python and send to the simulation engine via a UDP socket. It is assumed that the state of the AUV is known to the controller. In real-life experiments the correct localisation of the AUV with respect to the monopile is of the utmost importance. However, it is considered, for now, an adjacent problem.

In the numerical model, the quadratic drag on the AUV is computed using the cross-flow drag principle [14]. The hull is discretised into 75 strips, and the total drag force is obtained by integrating the contribution of each strip.

The generated CFD data was sampled at the mid-span of the monopile and reused in a one-way coupled way inside the dynamic simulation environment, i.e. the flow is assumed to be unaffected by the presence of the AUV, which is a reasonable assumption given the large difference in size between the monopile and the AUV. For every strip, the local flow field was interpolated from the CFD data, allowing the model to account for spatial variations in current velocity. This local-velocity approach was also needed when the AUV moved out of the monopile's wake. In such an instance, the bow may already be exposed to the higher current, while the aft section remains in the sheltered leeward region. Next, slender body theory has been used to calculate the hydrodynamic coupling between the degrees of motion, e.g. the hydrodynamic coefficients $X_{\mathrm{vr}}, Y_{\mathrm{uv}}, Y_{\mathrm{ur}}, N_{\mathrm{uv}}$ and $N_{|\mathrm{u}|\mathrm{l}}$ [15]. Finally, the added mass and the surge damping is used from previously reported free-sailing identification experiments [16]. The resulting equations can be written as a manouevring model [17] where the cross drag terms are calculated at every time-step of the integration.

The AUV under consideration is fully-actuated. This means that all degrees of freedom can be independently actuated. In order to focus on reduction of the repetitive disturbances, the thrusters are not explicitly modelled; a force and moment that act on the centre of gravity is used.

III. CONTROL

The AUV circles the $R = 5$ m radius monopile at a distance of one meter, maintaining a constant speed of $u_{\mathrm{sp}} = 0.5$ m/s. In normal operation, the AUV would gradually move upwards with each rotation to inspect the entire monopile, but in this study the motion has been restricted to the horizontal plane. The resulting trajectory therefore repeats each $t = 2\pi\ (5+1)/0.5 \approx 75.4$ s. The sideways looking camera remains oriented perpendicular to the monopile throughout the manouevre. The MAUV is fully actuated. Hence, the trajectory can be directly tracked without the need of guidance. The setpoints to these controllers describe the circumnavigation and are given as: $(x, y, \psi)_{\mathrm{sp}} = \left(\tilde{R}\sin(\psi_{\mathrm{sp}}), \tilde{R}\cos(\psi_{\mathrm{sp}}), tu_{\mathrm{sp}}/\tilde{R}\right)$, where $\tilde{R}$ denotes the radius of the trajectory, which equals the monopile's radius plus a 1 m stand-off.

An independent PID controller is used for each degree of freedom. The proportional- and differential gain are selected such that closed loop behaviour mimics a second order damped system:

$$K_{\mathrm{p}} = m\omega_{\mathrm{n}}^2, \quad (1)$$

$$K_{\mathrm{d}} = 2m\zeta\omega_{\mathrm{n}}. \quad (2)$$

All damping comes from the controller with these gains. The physical damping will further stabilise the control behaviour. In the equation m denotes the combination of rigid body mass and added mass for each DOF, ζ is the required relative damping, and ω_{n} is the selected natural frequency of the second order system. The relative damping used is $\zeta = 0.6$ for all DOF, the natural frequency is set to $(\omega_{\mathrm{n}}^x, \omega_{\mathrm{n}}^y, \omega_{\mathrm{n}}^\psi) = (2\pi/5, 2\pi/5, 2\pi/4)$ rad/s. The slightly larger bandwidth for the heading controller is needed to keep the prow into the

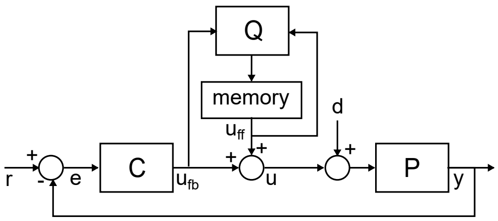

Fig. 6: Schematic view of Repetitive Control for a single degree of freedom. P and C represent the plant and controller respectively. An update to the feed forward signal u_{ff} is learnt from the feedback signal u_{fb}. The memory delays these signals for the duration of the circumnavigation.

current when the AUV leaves the leeward side of the monopile. The integral gain is selected for all DOFs as:

$$K_{\text{i}} = K_{\text{p}}^2/(NK_{\text{d}}), \tag{3}$$

with $N = 50$ such that the phase contribution at the 0-dB crossing is negligible, but steady state errors are removed.

Since the AUV completes each circuit around the monopile in a constant period, a time-dependent feed forward signal can be used to compensate for the repeatable, current-induced, disturbances. This signal can be learned directly from the feedback using Repetitive Control [6]. The concept is illustrated in Fig. 6. The lower-part of the picture shows a conventional control loop in which C depicts the controller, and P the plant. The feedback signal relates to this disturbance signal as:

$$\frac{u_{\text{fb}}}{d} = \frac{PC}{1+PC} \approx 1 \text{ when } \quad PC \gg 1. \tag{4}$$

Because the loop gain PC is typically much larger than one at low frequencies, the feedback signal effectively reflects the disturbance signal. Using the feedback signal as the feedforward input during the next circumnavigation allows the controller to cancel the disturbance before it produces an error.

The filter Q can be used to attenuate high-frequency components in the learned feedforward signal or, as done in this work, to blend only a fraction of the feedback signal into the next iteration:

$$u_{\text{ff}}^{i+1} = \alpha u_{\text{fb}}^{i} + u_{\text{ff}}^{i}, \tag{5}$$

with α empirically selected as 1/3. The superscript denotes the turn index.

IV. Results

Two simulations were performed. In the first, the AUV had to move to a fixed position and hold station. This was done to test the feedback controller and the general effect of the current. In the second simulation, the AUV repeatedly circumnavigated the monopile.

A. Station keeping

The AUV starts at $(x, y, \psi) = (10\text{m}, 0\text{m}, 0°)$ and moves to $(x, y, \psi) = (7.5\text{m}, 1\text{m}, 90°)$. This moves the AUV in the turbulent side of the monopile. Results are shown in Fig. 7.

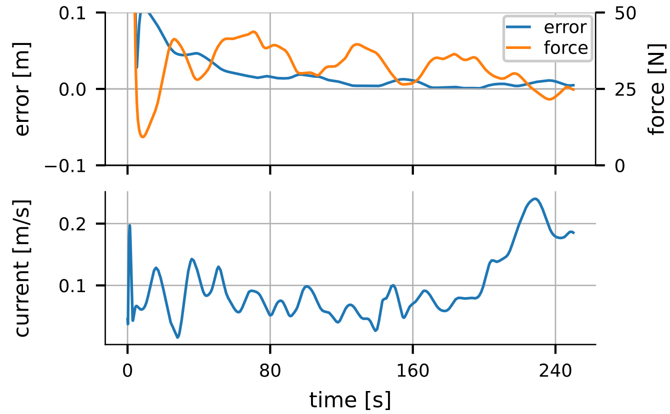

Fig. 7: Motion of the AUV to $(x, y, \psi) = (7.5\text{m}, 1\text{m}, 90°)$ where it has to maintain its position. The AUV is in the wake of the monopile perpendicular to the current.

The top-side of the figure shows the horizontal distance to the setpoint, as well as the feedback signal needed to maintain its position. The AUV is perpendicular to the current, and this force is hence exerted in the sway-direction of the vessel. The force in the surge-direction is much smaller.

The simulation shows that the AUV is capable of maintaining its position and heading in the turbulent flow with three decoupled PIDs as designed in section III. The force and force-rate during the station keeping are deemed acceptable to represent the actual behaviour of the mAUV, although it might be a bit on the fast side during transients. The overshoot of approximately 10 cm is slightly smaller than expected for a relative damping of $\zeta = 0.6$, but this can be contributed to the physical damping that was not included in the control design. Finally, the peak-peak error during station keeping is a few centimetres in the simulation.

The bottom-part of the figure shows the total current. As expected, it fluctuates and is smaller due to the shielding than the 0.5 m/s that was used as inflow. The next simulation shows the behaviour when the AUV has to sail a trajectory, which is more demanding on the controllers.

B. Circumnavigation

A bird-eye's view of the sailed path for the first three iterations are shown in Fig. 8. The white solid line denotes the reference path and the black line shows the sailed path in the shown iteration. Time traces are provided in Fig. 9 and Fig. 10 respectively. Two errors are shown in Fig. 9. The error shown by the blue line is the distance from the AUV to the location on the trajectory. As this measures a distance, it is always positive.

The second error, shown in orange, combines the horizontal errors and heading errors and is the error relevant for the sensor. It is the distance between the sensor and the spot it looks at on the monopile. The required distance of 1 m is subtracted from this distance to get the error. This error will be noted the sensor-distance error. Refer also to Fig. 5 for the symbols used. The distance from the sensor to the spot

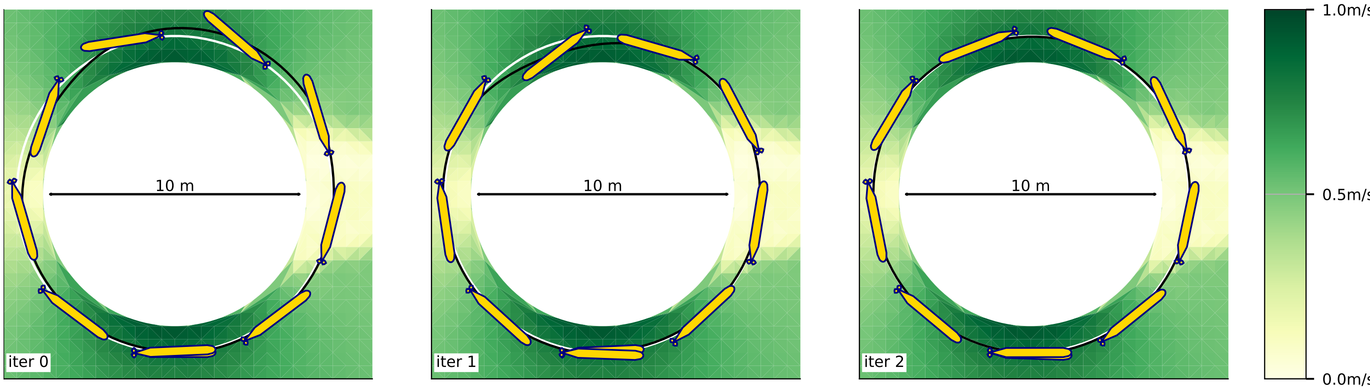

Fig. 8: The trajectory of the first three turns around the monopile. The white line is the reference path, and the black line shows the sailed path. The background shows the current field, ranging from 0.2 m/s to 0.8 m/s. The incoming current goes from left to right.

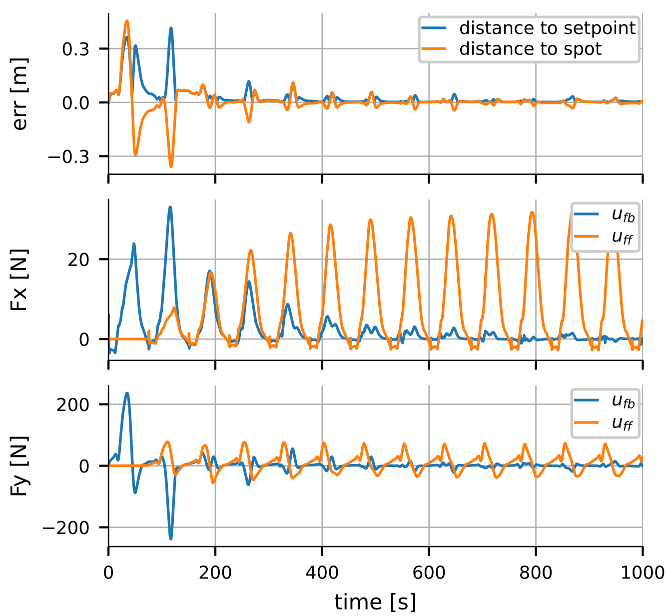

Fig. 9: The error and control signals during successive horizontal-plane circumnavigations. The blue curve shows the distance to the setpoint, whereas the orange trace reflects the camera-to-monopile distance at the point perpendicular to the vehicle, incorporating both horizontal-plane and heading errors. The bottom plots show the feedback and feed forward signals in ship-fixed coordinates in x- and y-direction.

perpendicular to it on the monopile is found via the cosine-rule as the smallest root of:

$$d^2 - d(2(R+l)\cos(\alpha)) + l^2 + 2Rl = 0. \tag{6}$$

Fig. 9 and 10 clearly show that the tracking error significantly reduces when the number of turns increases. The maximum absolute distance between the AUV and its setpoint reduces form 0.365 m to 0.011 m. The maximum absolute heading error starts at 20.8° and reduces to 0.56° in the 20$^{\text{th}}$ iteration. The sensor-distance error decreases from 0.455 m to 0.011 m. Because the trajectory is better followed, the largest deviation in the surge speed was in the first iteration found to be 0.44 m/s, and in the last 0.498 m/s.

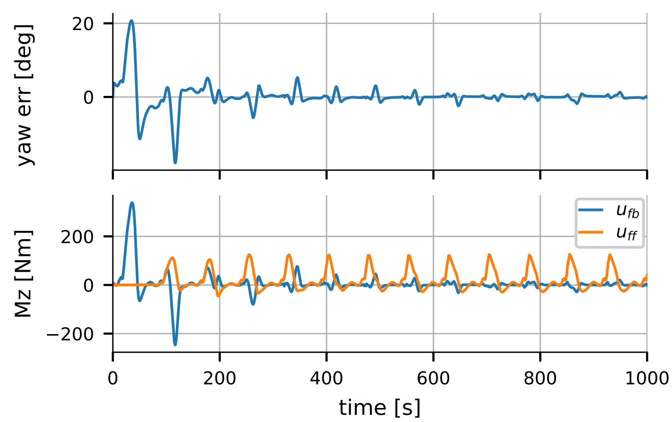

Fig. 10: The error and control signals for successive circumnavigations for the heading.

At the end of the simulation the contribution of the feed forward signal dominates the contribution of the feedback signal. This indicates that the majority of the disturbances are repetitive in nature. The remaining error correlates well with the error that was found for the station keeping. This stochastic part of the turbulence cannot be compensated for with feed forward and a feedback controller will always be necessary to cancel them.

It is interesting to note that the peak moment needed to circumnavigate the AUV is much *smaller* at the end than at the first iteration. At the first turn the bow breaks out when it comes out of the monopile's shielding. This can be seen in the top of Fig. 8. Because of this large deviation the feedback controller compensates with a large moment to bring it back to its setpoint. However, because of the feed forward signal, this deviation is avoided and hence the feedback controller does not need to provide such a large signal. Similar effects are not observed in the x- and y-direction.

Even if the errors for the individual degrees of freedom decrease, this does not guarantee safe operation for the system on the whole. This is illustrated in the second iteration in Fig. 8. The translational error brings the AUV closer to the monopile, while at the same time the rotational error brings the bow even closer. In the simulation there was no collision, but for real-life inspections one might want to increase the safety of the system by starting at a larger radius and decreasing it to the correct radius. This would require extra turns though.

The behaviour can be understood by looking at the control signals at the first two iterations. In the first iteration the feedback signal is large to counter the heading deviation. This signal is used as a feed forward signal in the second iteration. This steers the bow of the AUV through the current, which in its turn induces a large moment to the other direction and the accompanying overshoot. This has to be handled by the feedback controller. A smaller value of α in Eq. 5 would decrease the magnitude of this mechanism at the cost of slower convergence.

V. Discussion

A Repetitive Control scheme is used in this simulation to improve the tracking of an AUV for the inspection of a monopile. A turbulent wake field was first calculated by CFD and the local flow field was used in a cross-flow drag model to model the effect of this on the AUV's behaviour in the horizontal plane. The model further incorporated linear coupling terms from slender body theory, and added mass and surge damping from free-running experiments.

The Repetitive Control scheme used showed that information on the current run can be incorporated in the next turn to improve the tracking behaviour. The total lateral error decreased from 0.365 m to a few centimetres. The heading error improved from 20.8° to 0.56°.

Some assumptions were made to investigate the error reduction due to repetitive control. These assumptions will negatively impact the actual values provided, and are planned to be investigated further. The AUV's pose was to be assumed known. This is a strong assumption as localisation underwater is known to be a hard problem. We are interested in the relative pose with respect to the monopile. A sonar or a Doppler Velocity Log does provide these measurements. It does help that a monopile has a hard surface that will reflect the beams well. Still, among others, noise levels, sensor delays and systematic errors will decrease the performance.

Next to the sensors, the actuators were assumed perfect. The relation between RPM and generated thrust is influenced by the local current field as well as the position of the thruster with respect to the hull. To improve the performance and hence the safety, the requested thrust should match the generated thrust. Care should be taken to allocate the forces to the thrusters and probably include its uncertainty in the control design.

References

[1] T. Macquart, D. Kucukbahar, and B. Prinsen, "Dutch Offshore Wind Market Report 2023," Netherlands Enterprise Agency (RVO), Utrecht, The Netherlands, Tech. Rep., Apr. 2023.

[2] S. Pedersen, J. Liniger, M. Von Benzon, F. F. Sørensen, and C. Mai, "Towards Autonomous Subsea Maintenance on Offshore Structures with Unmanned Underwater Vehicles," in *OCEANS 2024 - Singapore*. Singapore, Singapore: IEEE, Apr. 2024, pp. 1–7.

[3] A. Lidtke, D. Rijpkema, and B. Düz, "General Reinforcement Learning Control for AUV Maneuvering in Turbulent Flows," *Applied Ocean Research*, vol. (submitted), 2024.

[4] N. Gu, D. Wang, Z. Peng, J. Wang, and Q.-L. Han, "Disturbance observers and extended state observers for marine vehicles: A survey," *Control Engineering Practice*, vol. 123, p. 105158, Jun. 2022.

[5] M. Von Benzon, J. Liniger, F. F. Sørensen, and S. Pedersen, "Investigation of Operating Range of Marine Growth Removing ROV under Offshore Disturbances," *IFAC-PapersOnLine*, vol. 55, no. 31, pp. 85–90, 2022.

[6] Y. Wang, F. Gao, and F. J. Doyle, "Survey on iterative learning control, repetitive control, and run-to-run control," *Journal of Process Control*, vol. 19, no. 10, pp. 1589–1600, Dec. 2009.

[7] K. Sunday and F. Brennan, "A review of offshore wind monopiles structural design achievements and challenges," *Ocean Engineering*, vol. 235, p. 109409, 2021.

[8] K. A. Schmoor and M. Achmus, "Optimum geometry of monopiles with respect to the geotechnical design," *J. Ocean Wind Energy*, vol. 2, no. 1, pp. 54–60, 2015.

[9] DHI A/S, "Metocean Desk Study and Database for Ten Noorden van de Waddeneilanden Wind Farm Zone," Webinar presentation prepared for the Netherlands Enterprise Agency (RVO), Apr. 2022, presented by Hendrik Wrenger, DHI A/S. [Online]. Available: https://offshorewind.rvo.nl/file/download/860a9e21-bcee-4361-ba1f-d3fa83a49e0c/tnw_20220330_dhi_metoceanwebinar_presentation_1.pdf

[10] F. Pereira, G. Vaz, L. Eça, and S. Girimaji, "Simulation of the flow around a circular cylinder at re= 3900 with partially-averaged navier-stokes equations," *International Journal of Heat and Fluid Flow*, vol. 69, pp. 234–246, 2018.

[11] A. K. Lidtke, M. Klapwijk, and T. Lloyd, "Scale-resolving simulations of a circular cylinder subjected to low mach number turbulent inflow," *Journal of Marine Science and Engineering*, vol. 9, no. 11, p. 1274, 2021.

[12] H. Cozijn, H. V. D. Schaaf, B. J. de Kruif, and E. Ypma, "Design of an Underwater Vehicle for use in Basin Experiments, Development of MARIN's Modular AUV," *IFAC-PapersOnLine*, vol. 52, no. 21, pp. 21–26, 2019.

[13] MARIN, "aNySIM XMF," https://www.marin.nl/en/facilities-and-tools/software/anysim, 2022.

[14] J. Hooft, "The cross-flow drag on a manoeuvring ship," *Ocean Engineering*, vol. 21, no. 3, pp. 329–342, Apr. 1994.

[15] J. N. Newman, "Applications of Slender-Body Theory in Ship Hydrodynamics," *Annual Review of Fluid Mechanics*, vol. 2, no. 1, pp. 67–94, Jan. 1970.

[16] B. J. de Kruif and E. Ypma, "Self-Propulsion Parameter Identification for Control of Marin's AUV," in *2020 IEEE/OES Autonomous Underwater Vehicles Symposium (AUV)(50043)*. IEEE, Sep. 2020, pp. 1–6.

[17] H. Yasukawa and Y. Yoshimura, "Introduction of MMG standard method for ship maneuvering predictions," *Journal of Marine Science and Technology*, vol. 20, no. 1, pp. 37–52, Mar. 2015.